Development of rear surface passivated Cu(In,Ga)Se$_2$ thin film solar cells with nano-sized local rear point contacts

CrossMark

Bart Vermang *, Viktor Fjällström, Jonas Pettersson, Pedro Salomé, Marika Edoff

Ångström Solar Center, University of Uppsala, P.O. Box 534, 75121 Uppsala, Sweden

ABSTRACT

For the first time, a novel rear contacting structure for copper indium gallium (di)selenide (CIGS) thin film solar cells is discussed theoretically, developed in an industrially viable way, and demonstrated in tangible devices. The proposed cell design reduces back contacting area by combining a rear surface passivation layer and nano-sized local point contacts. Atomic layer deposition (ALD) of Al$_2$O$_3$ is used to passivate the CIGS surface and the formation of nano-sphere shaped precipitates in chemical bath deposition (CBD) of CdS to generate point contact openings. The Al$_2$O$_3$ rear surface passivated CIGS solar cells with nano-sized local rear point contacts show a significant improvement in open circuit voltage (V_{OC}) compared to unpassivated reference cells. Comparing the passivated devices to solar cell capacitance simulator (SCAPS) modeling indicates that this increase is attributed to a decrease in rear surface recombination of a few orders.

© 2013 The Authors. Published by Elsevier B.V. Open access under CC BY-NC-SA license.

1. Introduction

World record solar cell efficiencies for thin film and silicon (Si) solar cells are respectively 19.6% and 25.0%, where best performing thin film technologies are based on CIGS absorber layers [1].

It is fair to say that a large part of this gap in world record cell efficiency between Si and CIGS technologies – which is even larger for record efficiencies achieved in the corresponding industries [2] – stems directly from their difference in cell design complexity. In Si PV industry, more advanced passivated emitter and rear cell (PERC) or passivated emitter rear locally-diffused (PERL) and analogous cell designs are being introduced to reach high efficiencies using ever thinner wafers [3,4]. Standard advances are the use of front and rear surface passivation layers, a selective emitter, and locally-diffused point contacts at the rear [4].

The rear of those advanced Si cell designs is improved by a combination of an adequate rear surface passivation stack and micron-sized local point contacts, which allows the use of thinner wafers – from 300 μm down to less than 200 μm – and improves the rear surface passivation and rear internal reflection significantly. A schematic representation of the rear of this p-type Si PERC design is shown in Fig. 1(a); the typical Si wafer thickness,

minority carrier diffusion length (L_n), contact opening diameter and distance between contact openings are specified [5–7]. Characteristic surface passivation layers for p-type Si are a combination of aluminum oxide (Al$_2$O$_3$), silicon oxide (SiO$_2$), and hydrogenated silicon nitride (SiN$_x$:H) [8,9], while the micron-sized openings are generated industrially by applying laser technology [7,10,11].

The purpose of this work is to apply this concept of rear surface passivation in an industrially viable way to CIGS solar cells. Therefore, an advanced cell design is developed to decrease the area of back contacting of CIGS solar cells combining a rear surface passivation layer and – since thin film solar cells have short minority carrier lifetimes and thus diffusion lengths – a technologically feasible approach to generate nano-sized local point contacts. This way, back contact recombination is reduced enabling higher efficiencies, particularly for ever thinner CIGS absorber layers – from 3 μm down to less than 1.5 μm. Hence, assuming L_n between 0.75 and 1.50 μm is feasible [12,13] the contact openings targeted are between 200 and 400 nm in diameter with internal spacing between 1.5 and 3.0 μm, as roughly deducted from the Si PERC design and shown in Fig. 1(b).

2. Material and methods

2.1. Material

A detailed description of CIGS solar cells fabricated in this work can be found in [14]; excluding the absorber layer formation and the advanced back contact design. The substrate used is low-iron soda lime glass (SLG) with a thickness of 1 mm. The back contact Mo layer
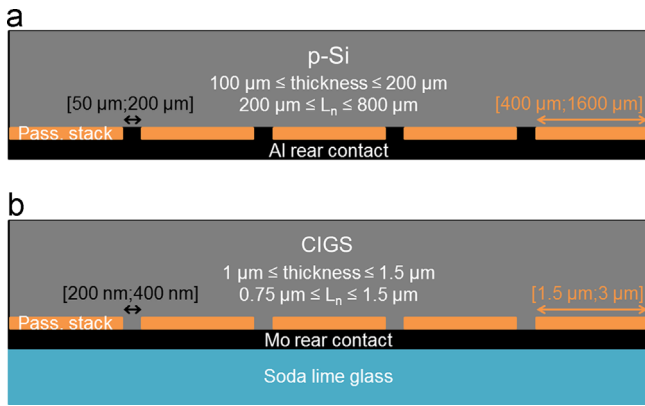

Fig. 1. Schematic representation of the rear of (a) a p-type Si solar cell with a surface passivation stack and micron-sized local point contacts and (b) a CIGS solar cell with a surface passivation stack and nano-sized local point contacts. Also the typical base/absorber thickness, minority carrier diffusion length, contact opening diameter and distance between contact openings are specified.

is deposited in an inline sputtering system, has a sheet resistance of $0.6 \, \Omega/\square$ and a typical thickness of 350 nm. The buffer layer is deposited using a standard CBD CdS process. The CBD CdS is grown at 60 °C in a solution with 1.136 M ammonia, 0.100 M thiourea and 0.003 M cadmium acetate. Next, the shunt reducing intrinsic ZnO layer (i-ZnO), and subsequently the Al-doped ZnO (ZnO:Al) front contact of the cells are sputtered. The (i-)ZnO(:Al) stack has a total thickness around 400 nm. The front contact grid is a Ni/Al/Ni stack deposited by evaporation through a shadow mask and its total thickness is around 3000 nm. Finally 0.5 cm^2 solar cells are defined by mechanical scribing with a stylus. No anti-reflective coating is used. Note that the back contact, absorber and buffer layer of all solar cells used in this manuscript are deposited in the same run. Only the transparent conductive oxide (TCO) is deposited separately for each type of device (because of throughput limitations), but its resistivity is monitored and kept equal for each cell.

The CIGS absorber layer is modified to the task: allowing the evaluation of an obvious improvement in V_{OC} if the rear surface passivation is enhanced. The CIGS layer is deposited in a high-vacuum chamber equipped with open-boat evaporation sources while evaporation rates are monitored using a mass spectrometer. During the CIGS growth, the substrate temperature is 540 °C, Se is evaporated in excess and constant rates of Cu, In and Ga are applied until the desired CIGS thickness is reached. All the studied samples have compositional values of [Cu]/([Ga]+[In])=0.84 ± 0.04 and [Ga]/([Ga]+[In])=0.27 ± 0.01, and thicknesses of 1.50 ± 0.02 μm. These 'flat-evaporation-rate-CIGS' absorbers with uniform low Ga concentration are favored to assess rear surface passivation, because of their high reproducibility, their characteristic high L_n [12], and to exclude any other rear surface passivation effects (e.g. a quasi-electrical field created by a Ga gradient causing a slope in the conduction band). This approach leads to cell efficiencies below 16.5%, but allows an evident boost in solar cell characterization results if the advanced CIGS cell design functions.

The advanced back contact design combines an ALD Al$_2$O$_3$ rear surface passivation layer and CBD of CdS to generate nano-sized local rear point contacts. The ALD Al$_2$O$_3$ passivation layers are deposited in a temporal ALD reactor at standard temperatures using trimethylaluminum (TMA) and ozone (O$_3$) as precursors; and the same CBD process as used for the CdS buffer layer is applied.

2.2. Methods

The [Cu]/([Ga]+[In]) and [Ga]/([Ga]+[In]) compositional values are calculated from X-ray fluorescence (XRF) measurements and film thicknesses are measured with a profilometer. Light

J–V-measurements are performed at 25 °C under standard AM1.5 G conditions in a home-made system with a tungsten halogen lamp, which is calibrated using a certified silicon photo diode. The CIGS solar cells are modeled using the latest version (3.2) of SCAPS [15,16], a list of parameter values used in the SCAPS modeling can be found in Appendix A. Rear internal reflection at the Mo/(CdS/Al$_2$O$_3$/)CIGS interface is calculated as in [17], applying thickness, refractive index and extinction coefficient of the Al$_2$O$_3$ layer as measured on a Si substrate using spectrally resolved ellipsometry.

3. Results and discussion

3.1. SCAPS modeling

The fabricated CIGS solar cells are modeled using SCAPS [15,16]. Fig. 2 depicts the variation in V_{OC} as a function of CIGS absorber layer thickness and rear surface recombination velocity (S_b, equivalent values are assumed for electron and hole recombination velocities) in case of a wavelength-independent rear internal reflection (R_b) of 70%. Fig. 3 represents the change in short circuit current (J_{SC}) as a function of CIGS absorber layer thickness and R_b, while S_b equals 1×10^3 cm/s – indicating a reasonable level of rear surface passivation. Note that the complementary solar cell characteristics for Figs. 2 and 3 can be found in Appendix B.
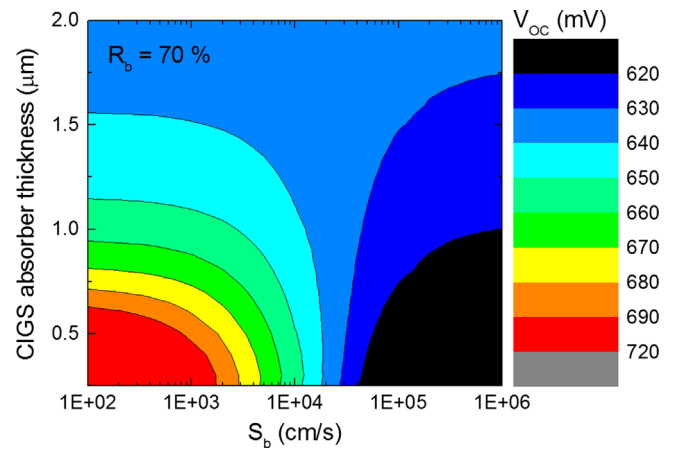

Fig. 2. Variation in open circuit voltage as a function of CIGS absorber layer thickness and rear surface recombination velocity, as simulated by SCAPS. The rear internal reflection is kept wavelength-independent and equals 70%.
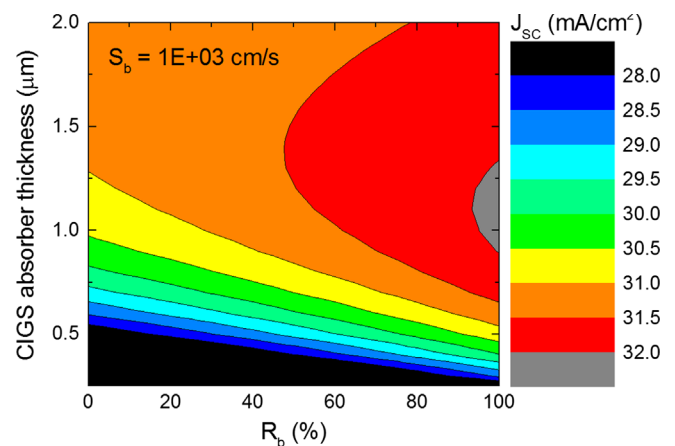

Fig. 3. Variation in short circuit current as a function of CIGS absorber layer thickness and rear internal reflection, as simulated by SCAPS. The rear surface recombination velocity is kept at 1×10^3 cm/s.

The SCAPS modeling shows that rear surface passivation of thin CIGS solar cells can lead to higher V_{OC} and J_{SC} – and hence cell efficiency – if the passivation layer supplies sufficient surface passivation and internal reflection at the same time. For $R_b=70\%$, Fig. 2 shows that using thinner CIGS absorber layers leads to higher V_{OC} if the S_b is low enough, e.g. $S_b=1\times10^3$ cm/s. However, as shown in Fig. 3, if a rear surface passivation layer leading to $S_b=1\times10^3$ cm/s is combined with CIGS absorber layers that are too thin and R_b that is too low, the absorption of charge carriers, and hence J_{SC}, will drop. Fortunately, combining CIGS absorber layers between 1 and 1.5 μm thick with a rear surface passivation leading to (i) low enough S_b ($\leq 1\times10^4$ cm/s; S_b of a typical Mo/CIGS interface is about 1×10^6 cm/s [18]) and (ii) high enough R_b ($\geq60\%$; typically $R_b\leq60\%$ for the Mo/CIGS interface, see below), does improve the CIGS solar cell V_{OC} and even J_{SC}.

3.2. Nano-sized point contacts and Al₂O₃ surface passivation

The technologically viable approach to generate nano-sized point contacts is based on the formation and subsequent removal of spherical particles (so-called colloids or precipitates) in CBD of CdS. After preparing the CBD solution, SLG/Mo substrates are only dipped when the CBD solution reacted for X min – during which time CdS particles are formed within the solution [19]. Thereafter, the substrates are immersed for Y min and a thin particle-rich CdS film is grown. By varying time intervals X and Y the particle-density can be varied. Fig. 4 shows scanning electron microscopy (SEM) pictures of thin particle-rich CdS layers deposited on SLG/Mo substrates before and after particle removal; in this case X and Y equal 4 min and an extra layer of CdS is grown to intensify the contrast in Fig. 4(b). Particle removal is established in various ways, via (i) ultra-sonic
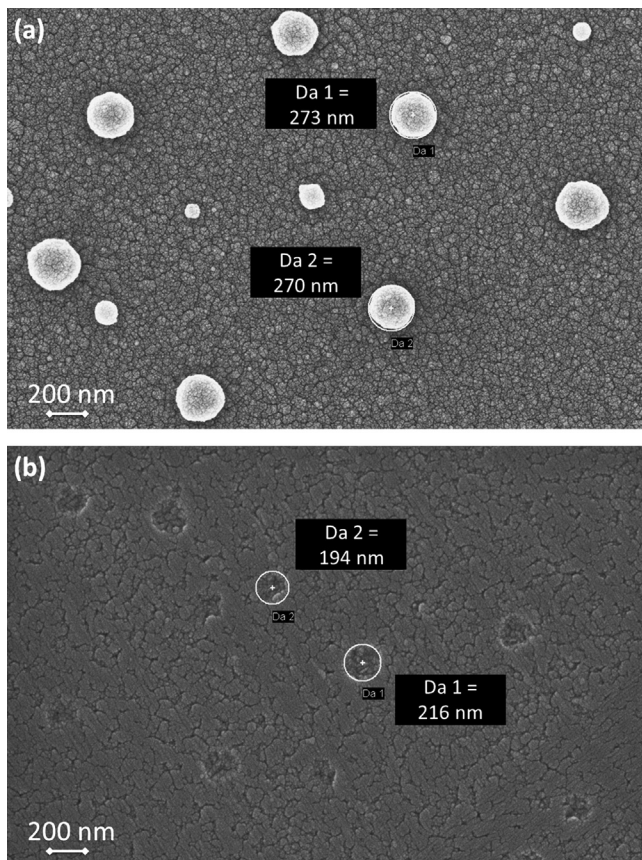

Fig. 4. Scanning electron microscopy pictures of (a) a particle-rich CdS layer grown on a SLG/Mo substrate and (b) the same substrate after CdS particle removal.
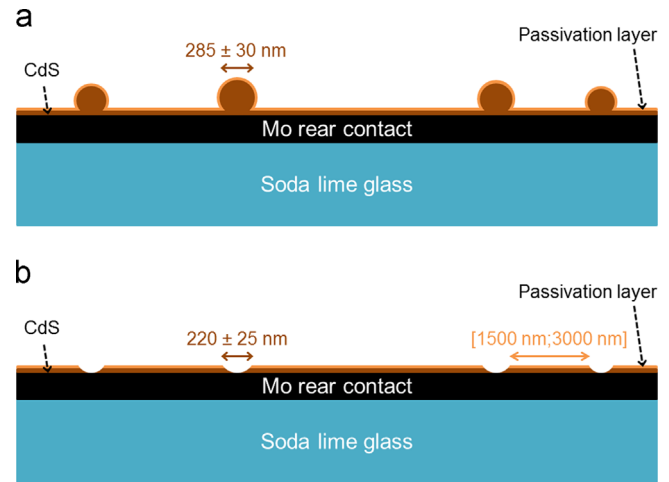

Fig. 5. Schematic cross-section of (a) a surface passivation layer grown on a particle-rich CdS layer, and (b) the full SLG/Mo/CdS/passivation-layer substrate having nano-sized point openings after CdS particle removal.

agitation, (ii) dry ice (liquid CO₂) cleaning, or (iii) mechanical wiping. Using SEM measurements, an average particle diameter of 285 ± 30 nm and average point opening diameter of 220 ± 25 nm is calculated.

To actually create nano-sized point openings in rear surface passivation layers for CIGS, the passivation layer is (a) grown on this particle-rich CdS layer and (b) subsequently the particles are removed; see Fig. 5 for a schematic representation. This way, a passivation layer with nano-sized point openings having a diameter around 220 nm is obtained.

ALD of Al₂O₃ is applied as CIGS surface passivation; it is an adequate passivation layer for p-type CIGS surfaces thanks to its high density of negative charges. Previously, an improvement of two orders in magnitude is reported for the integrated photoluminescence intensity of Al₂O₃ passivated CIGS compared to unpassivated CIGS: (i) first principles calculations indicate that the deposition of Al₂O₃ reduces about 35% of the interface defect density and (ii) Al₂O₃ exhibits a large density of negative charges – causing a field effect that reduces the CIGS surface minority charge carrier concentration and hence passivates the interface effectively [18].

3.3. Solar cell integration

Thick Al₂O₃ rear surface passivation layers are observed to blister during CIGS absorber layer evaporation, resulting in underperforming solar cells. Applying Al₂O₃ as rear surface passivation of CIGS solar cells implicates that the Al₂O₃ layer has to endure the harsh CIGS growth conditions: temperatures above 500 °C in an atmosphere of Se. Unfortunately, too thick ALD Al₂O₃ films annealed at such temperatures are observed to blister, deteriorating solar cell performance. Therefore, extremely thin films are applied: between 2 and 4 nm of Al₂O₃. However, this gives restrictions for R_b, as seen in Fig. 6 where R_b as a function of wavelength is depicted for an unpassivated CIGS device and 2 or 50 nm Al₂O₃ rear passivated CIGS devices. Fig. 6 shows that applying 2 nm of Al₂O₃ as rear surface passivation layer increases the R_b only slightly, a thicker Al₂O₃ layer or other approaches are needed for a larger R_b enhancement. Note that blistering of Al₂O₃ and its negative impact on solar cell performance are also described earlier [8,20].

Since Al₂O₃ layers act as a barrier for Na diffusion from the SLG substrate, extra supply of Na is needed. Fig. 7 depicts representative J–V curves for Al₂O₃ (2 nm) rear surface passivated CIGS solar cells having nano-sized local rear point contacts with and without 15 nm of NaF evaporated on top of the Al₂O₃ passivation layer.

Fig. 7 shows that Al_2O_3 rear passivated cells without extra Na supply have a low fill factor (FF) and a J–V curve showing a "roll-over" effect, characteristic for devices lacking Na [21]. Note that (i) Al_2O_3 films are indeed known to be excellent gas diffusion barriers [20,22] and (ii) this roll-over effect is not as pronounced as in Na-free cells [21]. Furthermore, Fig. 7 also shows representative J–V curves for Al_2O_3 (2 nm) rear passivated CIGS solar cells without local rear point contacts and unpassivated reference cells.

Thin Al_2O_3 rear passivated CIGS solar cells (1.5 μm absorber thickness) with and without nano-sized local rear point contacts are made and compared to unpassivated reference cells, see Table 1 for an overview of the average solar cell characteristics. The large
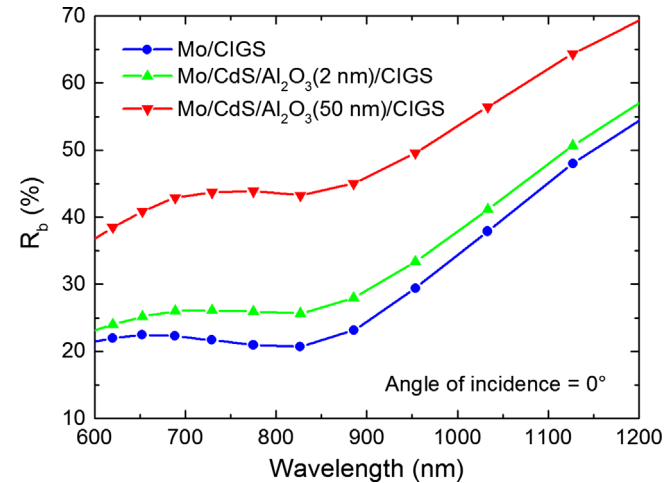

Fig. 6. Calculated rear internal reflection as a function of wavelength for a Mo/CdS/Al_2O_3(2 or 50 nm)/CIGS device or an unpassivated reference [17].
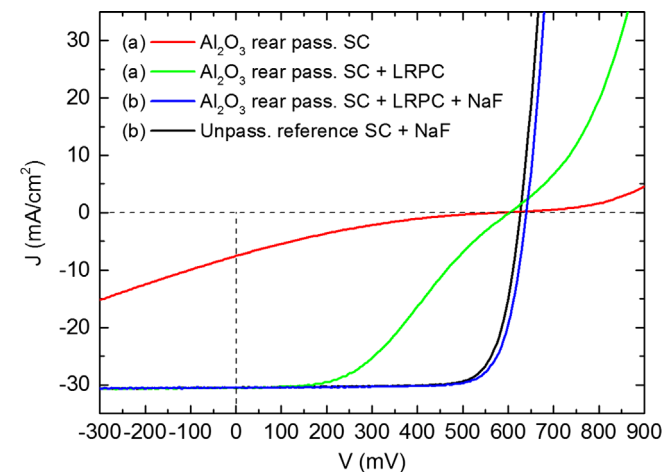

Fig. 7. Representative J–V curves for (a) Al_2O_3 (2 nm) rear surface passivated CIGS solar cells (SC) with and without nano-sized local rear point contacts (LRPC) and (b) Al_2O_3 rear passivated cells having nano-sized local rear point contacts and unpassivated reference cells with 15 nm of NaF evaporated on top of the Al_2O_3 or Mo layer, respectively.

difference in J_{SC} and FF between Al_2O_3 rear passivated cells with and without local rear point contacts (i) indicates that the passivation layer is intact after CIGS processing and (ii) proves that the point contacts are required to obtain appropriate back contacting. Thus, in other words, the Al_2O_3 film acts as a barrier layer for charge transport and therefore point openings are needed for back contacting. As listed in Table 1, the Al_2O_3 rear passivated solar cells with local rear point contacts show an average improvement in V_{OC} of 14 mV compared to the reference cells, while the average J_{SC}, FF and conversion efficiency (Eff.) results are comparable. For all cells listed in Table 1, a representative J–V curve can be found in Fig. 7. Note that for reasons of comparison also the unpassivated reference cells have an additional NaF layer (15 nm) deposited on the Mo back contact. However, unpassivated reference cells without this extra NaF layer lead to equivalent cell characteristics (not shown), which is expected as the used soda lime glass substrates contain plenty of Na.

The higher V_{OC}, but similar J_{SC} for Al_2O_3 rear surface passivated solar cells with nano-sized local rear point contacts compared to unpassivated reference cells can be explained by (a) improved rear surface passivation and (b) equivalent rear internal reflection. (a) Comparing SCAPS modeling to the manufactured solar cell devices indicates that the increase in V_{OC} is attributed to a decrease in rear surface recombination of a few orders. Fig. 8 shows the SCAPS simulated V_{OC} as a function of S_b for a CIGS absorber thickness of 1.5 μm and R_b as defined in Fig. 6. Also the solar cell devices having $V_{OC} \geq 628$ mV are shown in Fig. 8; it indicates that for Al_2O_3 rear passivated cells with local rear point contacts the minimal and average S_b are respectively 1×10^2 and 6.9×10^3 cm/s, while for the unpassivated reference cells the minimal and average S_b are 3×10^4 and 8.1×10^5 cm/s, respectively. These averages in S_b are also listed in Table 1. Note that a direct link between V_{OC} and rear surface passivation is assumed, because in case of adding NaF or a rear surface passivation layer no direct impact could be observed on solar cell characteristics for the unpassivated reference cells or on CIGS
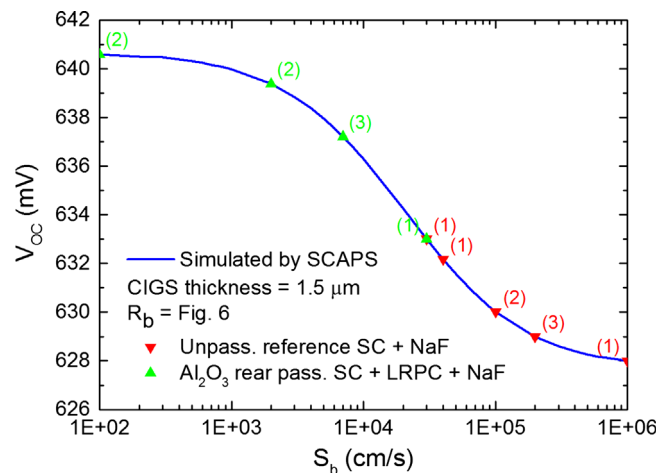

Fig. 8. SCAPS simulated open circuit voltage as a function of surface recombination velocity for a CIGS thickness of 1.5 μm and a rear internal reflection as defined in Fig. 6. Also the solar cell devices of Table 1 with $V_{OC} \geq 628$ mV are shown, and the quantity of devices having this specific V_{OC} is displayed between brackets.

Table 1
Overview of the average cell characterization results (AM1.5 G) and correlated rear surface recombination velocity (as modeled by SCAPS) for 0.5 cm² unpassivated reference CIGS solar cells and Al_2O_3 rear passivated cells with and without nano-sized local rear point contacts. For the cell results the standard deviation is also given.

Cell type	# Cells	V_{OC} (mV)	J_{SC} (mA/cm²)	FF (%)	Eff. (%)	S_b (cm/s)
Unpass. reference SC+NaF	32	624 ± 4	30.5 ± 0.4	78.5 ± 0.5	14.9 ± 0.3	8.1×10^5
Al_2O_3 rear pass. SC	8	534 ± 31	3.9 ± 1.6	16.0 ± 0.8	0.3 ± 0.2	N.A.
Al_2O_3 rear pass. SC+LRPC+NaF	8	638 ± 3	30.0 ± 0.6	78.8 ± 0.3	15.1 ± 0.4	6.9×10^3

microstructure (based on various cross-sectional SEM pictures), respectively. (b) The similar J_{SC} for the passivated and unpassivated solar cells is explained by a too small increase in R_b for adding a 2 nm Al_2O_3 rear surface passivation layer, as already seen in Fig. 6.

4. Conclusions and outlook

A rear surface passivation layer with nano-sized local rear point contacts is demonstrated in thin film CIGS solar cells. ALD of Al_2O_3 is used to passivate the CIGS surface and the formation of nano-sphere shaped precipitates in chemical bath deposition of CdS to generate point contact openings. A 2 nm ALD Al_2O_3 surface passivation layer with local point openings of about 220 nm is used to improve the rear surface passivation of CIGS solar cells having 1.5 μm thick absorber layers. An increase in average V_{OC} of 14 mV is observed compared to unpassivated reference cells, thanks to a decrease in rear surface recombination of a few orders. The minimal S_b for the Al_2O_3 rear passivated and unpassivated CIGS solar cells are 1×10^2 and 3×10^4 cm/s, respectively.

However, to obtain the full potential of this advanced rear contacting design more reflective rear surface passivation layers have to be combined with even thinner CIGS absorber layers and a more optimized point contacting grid. In Figs. 2 and 3, it is shown that – if R_b is high enough – additional improvement of V_{OC} and even J_{SC} can be expected for cells with a 1 μm thick absorber layer. Therefore, the attention is currently on (i) developing an approach to use thicker Al_2O_3 films (see Fig. 6 for the impact of Al_2O_3 thickness on R_b), (ii) integrating other advanced light trapping techniques (e.g. [23]) and (iii) screening other passivation layer candidates. Moreover, the present contact opening configuration is based on rough calculations. Therefore, other technologically feasible contact opening approaches are investigated in combination with ideal contacting grids created by electron beam lithography. A variation in contacting grids can then be used to investigate the influence of CIGS grain boundaries, which is currently omitted in the applied 1-D SCAPS modeling [24].

Acknowledgments

Appendix A

Scheme A.1 List of parameters used in SCAPS modeling. For more details, see [16].

CIGS layer
  Thickness=1.5 μm
  $N_a = 4 \times 10^{15}$ cm^{-3}
  Ga/(Ga+In)=0.27; $E_g = 1.15$ eV
  $\mu_e = 100$ cm^2/Vs
  $\mu_h = 12.5$ cm^2/Vs
  Deep donor defect
    $N_D = 9 \times 10^{13}$ cm^{-3}
    $\sigma_e = 1 \times 10^{-13}$ cm^2
    $\sigma_h = 1 \times 10^{-15}$ cm^2
    Single level, mid-gap

CIGS/CdS-interface
  Conduction band offset=0.19 eV

Deep donor defect
  $N_D = 9 \times 10^{12}$ cm^{-2}
  $\sigma_e = 1 \times 10^{-13}$ cm^2
  $\sigma_h = 1 \times 10^{-15}$ cm^2
  Single level, CIGS mid-gap

CdS layer
  Thickness=70 nm
  $N_d = 5 \times 10^{17}$ cm^{-3}
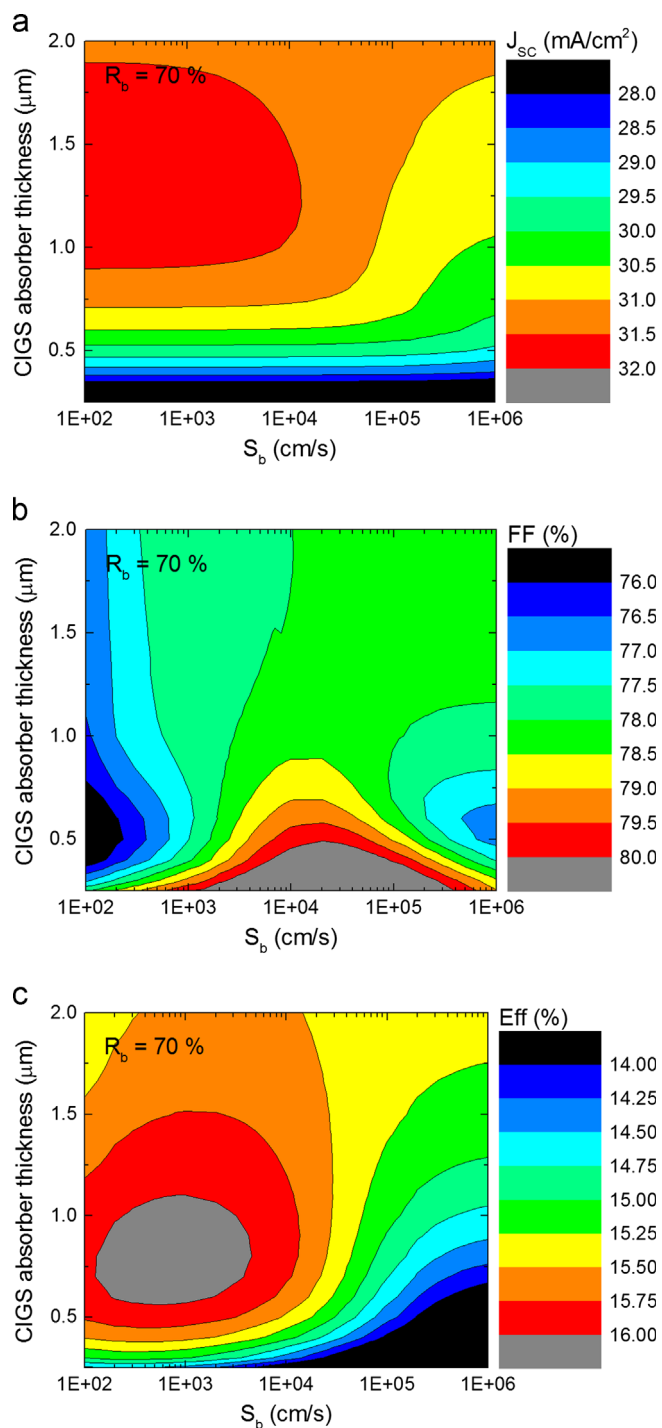 $E_g = 2.4$ eV
  Deep acceptor defect

Fig. B.1. Variation in J_{SC}, FF and Eff. as a function of CIGS absorber layer thickness and rear surface recombination velocity, as simulated by SCAPS. The rear internal reflection is kept wavelength-independent and equals 70%.
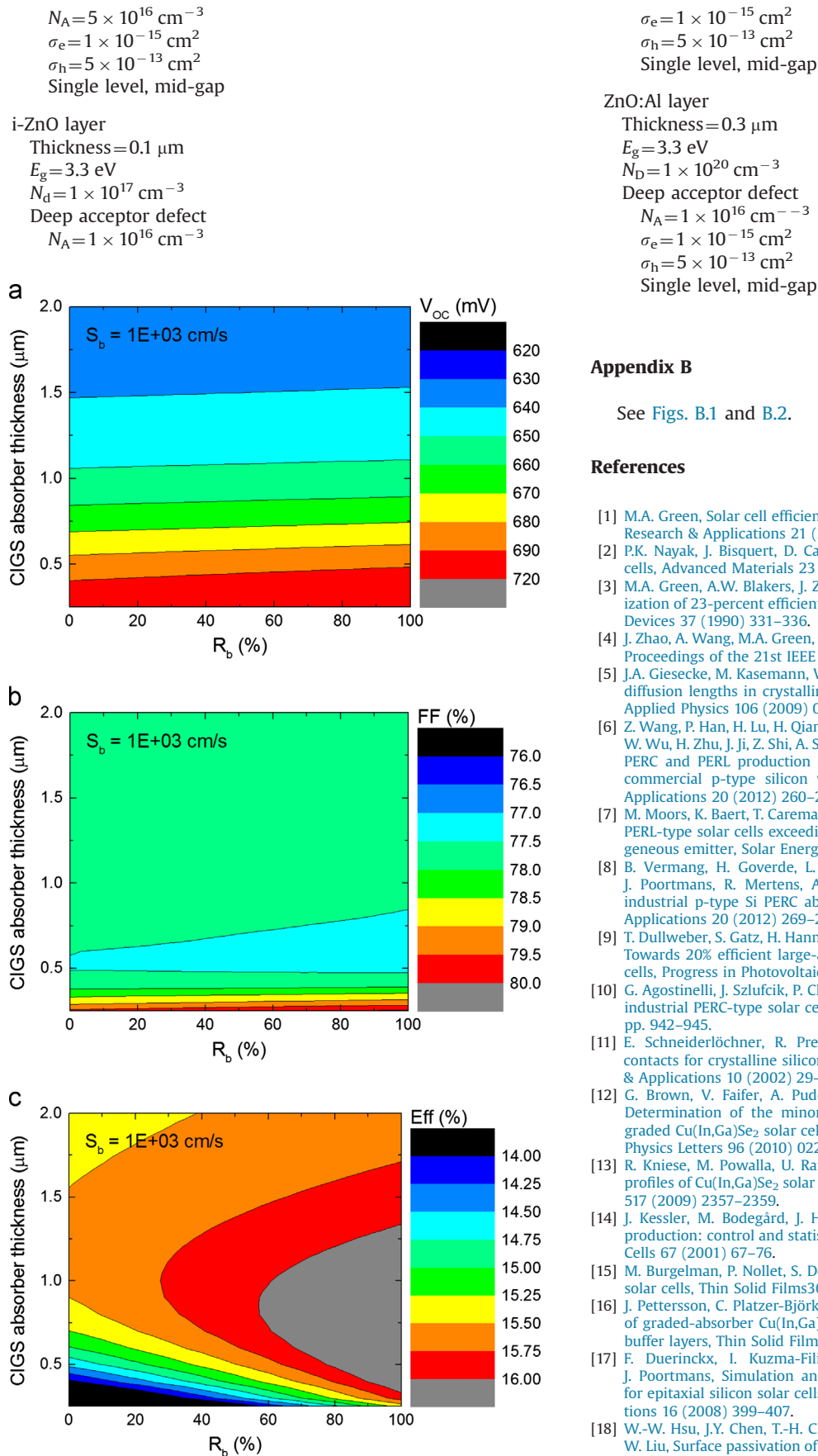
$N_A = 5 \times 10^{16}$ cm^{-3}
$\sigma_e = 1 \times 10^{-15}$ cm^2
$\sigma_h = 5 \times 10^{-13}$ cm^2
Single level, mid-gap

i-ZnO layer
    Thickness$=0.1$ μm
    $E_g = 3.3$ eV
    $N_d = 1 \times 10^{17}$ cm^{-3}
    Deep acceptor defect
      $N_A = 1 \times 10^{16}$ cm^{-3}

$\sigma_e = 1 \times 10^{-15}$ cm^2
$\sigma_h = 5 \times 10^{-13}$ cm^2
Single level, mid-gap

ZnO:Al layer
    Thickness$=0.3$ μm
    $E_g = 3.3$ eV
    $N_D = 1 \times 10^{20}$ cm^{-3}
    Deep acceptor defect
      $N_A = 1 \times 10^{16}$ cm^{--3}
      $\sigma_e = 1 \times 10^{-15}$ cm^2
      $\sigma_h = 5 \times 10^{-13}$ cm^2
    Single level, mid-gap

Appendix B

See Figs. B.1 and B.2.

Fig. B.2. Variation in V_{OC}, FF and Eff. as a function of CIGS absorber layer thickness and rear internal reflection, as simulated by SCAPS. The rear surface recombination velocity is kept at 1×10^3 cm/s.

References

[1] M.A. Green, Solar cell efficiency tables (version 41), Progress in Photovoltaics: Research & Applications 21 (2013) 1–11.
[2] P.K. Nayak, J. Bisquert, D. Cahen, Assessing possibilities and limits for solar cells, Advanced Materials 23 (2011) 2870–2876.
[3] M.A. Green, A.W. Blakers, J. Zhao, A.M. Milne, A. Wang, D. Ximing, Characterization of 23-percent efficient silicon solar cells, IEEE Transactions on Electron Devices 37 (1990) 331–336.
[4] J. Zhao, A. Wang, M.A. Green, 24% Efficient PERL structure silicon solar cells, in: Proceedings of the 21st IEEE PVSC, 1990, pp. 333–335.
[5] J.A. Giesecke, M. Kasemann, W. Warta, Determination of local minority carrier diffusion lengths in crystalline silicon from luminescence images, Journal of Applied Physics 106 (2009) 014907–014907-8.
[6] Z. Wang, P. Han, H. Lu, H. Qian, L. Chen., Q. Meng, N. Tang, F. Gao, Y. Jiang, J. Wu, W. Wu, H. Zhu, J. Ji, Z. Shi, A. Sugianto, L. Mai., B. Hallam, S. Wenham, Advanced PERC and PERL production cells with 20.3% record efficiency for standard commercial p-type silicon wafers, Progress in Photovoltaics: Research & Applications 20 (2012) 260–268.
[7] M. Moors, K. Baert, T. Caremans, F. Duerinckx, A. Cacciato, J. Szlufcik, Industrial PERL-type solar cells exceeding 19% with screen-printed contacts and homogeneous emitter, Solar Energy Materials & Solar Cells 106 (2012) 84–88.
[8] B. Vermang, H. Goverde, L. Tous, A. Lorenz, P. Choulat, J. Horzel, J. John, J. Poortmans, R. Mertens, Approach for Al$_2$O$_3$ rear surface passivation of industrial p-type Si PERC above 19%, Progress in Photovoltaics: Research & Applications 20 (2012) 269–273.
[9] T. Dullweber, S. Gatz, H. Hannebauer, T. Falcon, R. Hesse, J. Schmidt, R. Brendel, Towards 20% efficient large-area screen-printed rear-passivated silicon solar cells, Progress in Photovoltaics: Research & Applications 20 (2012) 630–638.
[10] G. Agostinelli, J. Szlufcik, P. Choulat, G. Beaucarne, Local contact structures for industrial PERC-type solar cells, in: Proceedings of the 20th EU PVSEC, 2005, pp. 942–945.
[11] E. Schneiderlöchner, R. Preu, R. Lüdemann, S.W. Glunz, Laser-fired rear contacts for crystalline silicon solar cells, Progress in Photovoltaics: Research & Applications 10 (2002) 29–34.
[12] G. Brown, V. Faifer, A. Pudov, S. Anikeev, E. Bykov, M. Contreras, J. Wu, Determination of the minority carrier diffusion length in compositionally graded Cu(In,Ga)Se$_2$ solar cells using electron beam induced current, Applied Physics Letters 96 (2010) 022104–022104-3.
[13] R. Kniese, M. Powalla, U. Rau, Evaluation of electron beam induced current profiles of Cu(In,Ga)Se$_2$ solar cells with different Ga-contents, Thin Solid Films 517 (2009) 2357–2359.
[14] J. Kessler, M. Bodegård, J. Hedström, L. Stolt, Baseline Cu(In,Ga)Se$_2$ device production: control and statistical significance, Solar Energy Materials & Solar Cells 67 (2001) 67–76.
[15] M. Burgelman, P. Nollet, S. Degrave, Modelling polycrystalline semiconductor solar cells, Thin Solid Films361–362 (2000) 527–532.
[16] J. Pettersson, C. Platzer-Björkman, U. Zimmermann, M. Edoff, Baseline model of graded-absorber Cu(In,Ga)Se$_2$ solar cells applied to cells with Zn$_{1-x}$Mg$_x$O buffer layers, Thin Solid Films 519 (2011) 7476–7480.
[17] F. Duerinckx, I. Kuzma-Filipek, K. Van Nieuwenhuysen, G. Beaucarne, J. Poortmans, Simulation and implementation of a porous silicon reflector for epitaxial silicon solar cells, Progress in Photovoltaics: Research & Applications 16 (2008) 399–407.
[18] W.-W. Hsu, J.Y. Chen, T.-H. Cheng, S.C. Lu, W.-S. Ho, Y.-Y. Chen, Y.-J. Chien, C.W. Liu, Surface passivation of Cu(In,Ga)Se$_2$ using atomic layer deposited Al$_2$O$_3$, Applied Physics Letters 100 (2012) 023508–023508-3.
[19] R. Ortega-Borges, D. Lincot, Mechanism of chemical bath deposition of cadmium sulfide thin films in the ammonia–thiourea system, Journal of the Electrochemical Society 140 (1993) 3464–3473.

[20] B. Vermang, H. Goverde, V. Simons, I. De Wolf, J. Meersschaut, S. Tanaka, J. John, J. Poortmans, R. Mertens, A study of blister formation in ALD Al_2O_3 grown on silicon, in: Proceedings of the 38th IEEE PVSC, 2012, pp. 1135–1138.

[21] P. Salomé, V. Fjällström, A. Hultqvist, M. Edoff, Na doping of CIGS solar cells using low sodium-doped Mo layer, IEEE Journal of Photovoltaics 3 (2013) 509–513.

[22] D. Bae, S. Kwon, J. Oh, W.K. Kim, H. Park, Investigation of Al_2O_3 diffusion barrier layer fabricated by atomic layer deposition for flexible $Cu(In,Ga)Se_2$ solar cells, Renewable Energy 55 (2013) 62–68.

[23] H. Tan, R. Santbergen, A.H.M. Smets, M. Zeman, Plasmonic light trapping in thin-film silicon solar cells with improved self-assembled silver nanoparticles, Nano Letters 12 (2012) 4070–4076.

[24] M. Nerat, Copper–indium–gallium–selenide (CIGS) solar cells with localized back contacts for achieving high performance, Solar Energy Materials & Solar Cells 104 (2012) 152–158.